RARE METALS

Anisotropy of two-dimensional ReS$_2$ and advances in its device application

Ya-Di Cao, Ying-Hui Sun* , **Su-Fei Shi, Rong-Ming Wang***

Abstract Two-dimensional (2D) transition metal dichalcogenides (TMDCs) have attracted growing interest regarding their potential applications in next-generation electronic and optoelectronic devices. Owing to their atomic thickness and tunable bandgap, they exhibit unique mechanical, electrical, and optical properties. As a specific member of the TMDC family, rhenium disulfide (ReS$_2$) has stimulated intensive interest due to its anisotropic crystal structure, weak inter-layer coupling, and anisotropic electrical and optical properties. In this review, we summarize the distinct crystal structure and intrinsic anisotropic properties of ReS$_2$, followed by an introduction to its synthesis methods. The current applications of ReS$_2$ and its heterojunctions are presented based on its anisotropic properties. This review not only provides a timely summary of the current applications of ReS$_2$ and its heterojunctions, but also inspires new approaches to develop other innovative devices based on 2D materials with a low lattice symmetry.

Y.-D. Cao, Y.-H. Sun*, R.-M. Wang*
Beijing Advanced Innovation Center for Materials Genome Engineering, Beijing Key Laboratory for Magneto-Photoelectrical Composite and Interface Science, School of Mathematics and Physics, University of Science and Technology Beijing, Beijing 100083, China
e-mail: yhsun@ustb.edu.cn

R.-M. Wang
e-mail: rmwang@ustb.edu.cn

S.-F. Shi
Department of Chemical and Biological Engineering, Rensselaer Polytechnic Institute, Troy, NY 12180, USA

S.-F. Shi
Department of Electrical, Computer and Systems Engineering, Rensselaer Polytechnic Institute, Troy, NY 12180, USA

1 Introduction

Two-dimensional (2D) transition metal dichalcogenides (TMDCs) are emerging semiconductor materials on account of their specific layered crystal structures and unique mechanical, optical, and electrical properties. The molecular formula of TMDCs is MX$_2$, where M is the transition metal element and X is the chalcogen element. The M atomic layer is sandwiched between two X atomic layers to form a three-layer covalent bonding unit, with the layers stacked vertically by the interaction of van der Waals forces. Two appealing aspects of the structure of TMDCs, leading to unique layer-related physical properties [1–4], are the strong in-plane covalent bonds and relatively weak out-of-plane van der Waals interactions. Furthermore, TMDCs have intrinsic and tunable bandgaps in the range of 1–2 eV [5–9], surpassing graphene which lacks a band gap [10]. The relatively high carrier mobility, high on–off ratio, high photoluminescence (PL) efficiency, and high binding energy of excitons in TMDCs could potentially lead to novel electronic and optoelectronic applications, including field-effect transistors (FETs), sensors, photodetectors [11, 12], and photocatalysis. In widely studied TMDCs, such as MoS$_2$, the electrical and optical properties are irrelevant to the orientation of the crystal axis in-plane because of the isotropic symmetrical structures. The transition from an indirect bandgap in the bulk material to a direct bandgap in monolayers occurs due to the interlayer coupling and 2D quantum confinement

effect. There have been a few studies of the anisotropic properties of TMDCs in relation to the anisotropic orientation of the crystal axis in-plane [13].

As a typical anisotropic 2D material, black phosphorus (BP) has different physical and chemical properties along the zigzag and armchair directions due to the in-plane anisotropic atomic arrangement [14–17]. The Young's modulus along the zigzag direction is about four times the value along the armchair direction, showing a strong anisotropy of internal stress [18, 19]. The angular-dependent PL spectrum also shows obviously anisotropic results [20, 21]. In view of these anisotropic characteristics of BP, the interest has been paid to other TMDCs with low structural symmetry.

It has been reported that 1T′ phase MoS_2, with an asymmetric structure, has in-plane anisotropic optical, electrical, and electrocatalytic properties [22]. The Raman spectrum shows a distinct anisotropic orientation-related result, which is in good agreement with the measurement of the angle-resolved charge transport. Its electrocatalytic activity has a definite dependence on the anisotropic charge transport. Additionally, the Raman and PL spectra of rhenium diselenide ($ReSe_2$) also display anisotropic characteristics [23–25]. Unlike other 2D TMDCs, the extremely weak interlayer bonding in addition to the low crystal symmetry of ReS_2 leads to a direct bandgap independent of the thicknesses [26, 27]. The unique crystal lattice, with one-dimensional (1D) in-plane Re–Re metallic chains, suggests a strong potential for the use of ReS_2 in novel 2D FETs, sensors, photodetectors, logic devices, and electrocatalysis reactions with anisotropic properties. It is therefore essential to review the anisotropic characteristics and the device applications based on ReS_2 and its heterostructures.

In this review, the anisotropic crystal structures, optical properties, and thermal conductivity of ReS_2 were summarized (Fig. 1), followed by its synthesis methods. We considered the electronic and optoelectronic applications of ReS_2 based on its highly anisotropic properties. Finally, we present the potentials and challenges for future research in this field. 2D ReS_2, with strong anisotropy as a fundamental property, can not only provide a new way to optimize the performance of functional devices, but may also inspire exotic ideas for the future development of devices.

2 Fundamental properties of ReS₂

2.1 Anisotropic crystal structure

Transition metal dichalcogenides typically have five phases, namely 2H, 3R, 1T, 1T′, and T_d [28], as shown in Fig. 2, where T, H, and R represent octahedral, hexagonal,
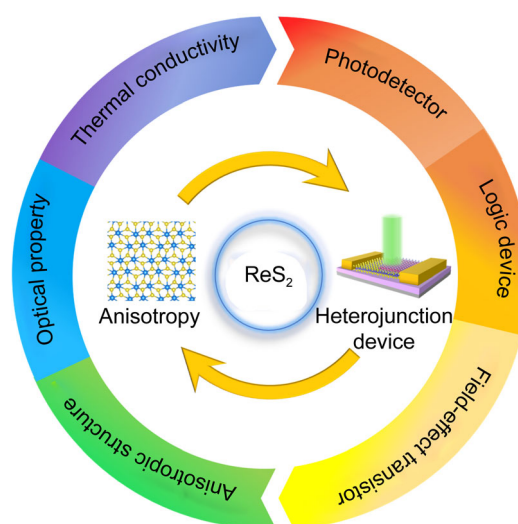

Fig. 1 Schematic illustration of outline of this review, including anisotropic properties and applications of ReS_2 and its heterostructures

and rhombic structures, respectively [28, 29]. The 2H and 1T phases are the basic phases of TMDCs. The 2H phase can be obtained by superimposing the monolayer of the H phase in the stacking sequence of ABA, which is a triangular prism with hexagonal symmetry [30]. The coordination mode of the 3R phase is the same as that of the 2H phase, but the stacking sequence is ABC [30]. The unit cell of the 1T phase is octahedral in coordination with tetragonal symmetry, and the repeating unit has only one layer. Owing to the thermodynamic instability of the 1T phase, it evolves into two deformations, i.e., the distorted octahedron (T′) and the trapezium phase (T_d, at low temperature and high pressure [31]) [32]. The 1T′ phase has lower in-plane symmetry, which is conducive to the unique anisotropic characteristics.

The in-plane symmetric crystal structures are usually responsible for the isotropic properties of TMDCs. For example, MoS_2 has a typical symmetric crystal structure, as shown in Fig. 3a [26]. The optical properties of MoS_2, such as its PL and Raman spectra, show a strong dependence on layer number [6, 33], but no characteristics related to its crystal orientation in-plane have been reported. In such 2D materials, with isotropic symmetrical structures, the electrical and optical properties are irrelevant to the orientation of the crystal axis, and therefore, the anisotropic properties are negligible.

Rhenium disulfide has a 1T′ phase, with a twisted octahedron structure that differs from the 1H structure of MoS_2. Each unit cell contains four Re atoms and eight S atoms. There are both metal–chalcogen and metal–metal bonds in ReS_2, and the length of every Re-S bond is different, as shown in Fig. 3a [34, 35]. Each Re atom
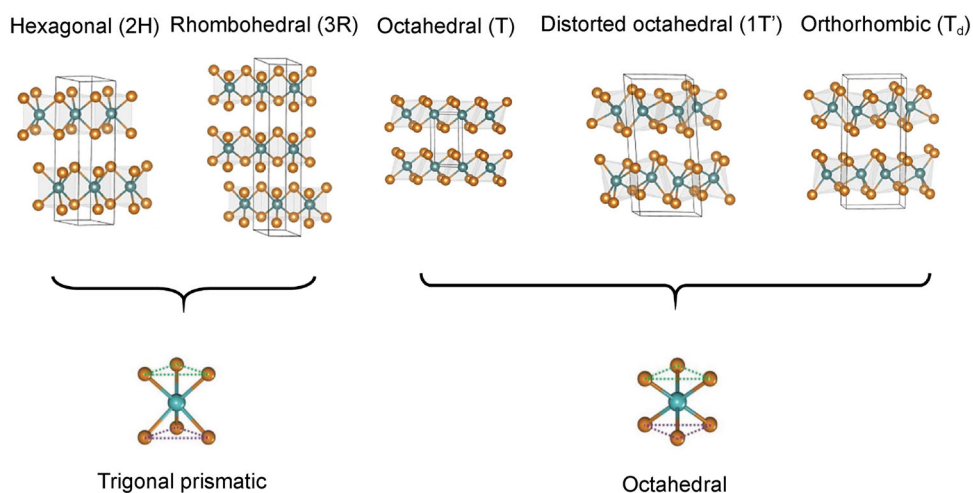
Fig. 2 Schematic illustration of atomic structure, bonding, and stacking modes of five phases in TMDCs (transition metal atoms in blue and sulfur atoms in light brown). Reprinted with permission from Ref. [28]. Copyright 2018 WILEY–VCH Verlag GmbH & Co. KGaA, Weinheim
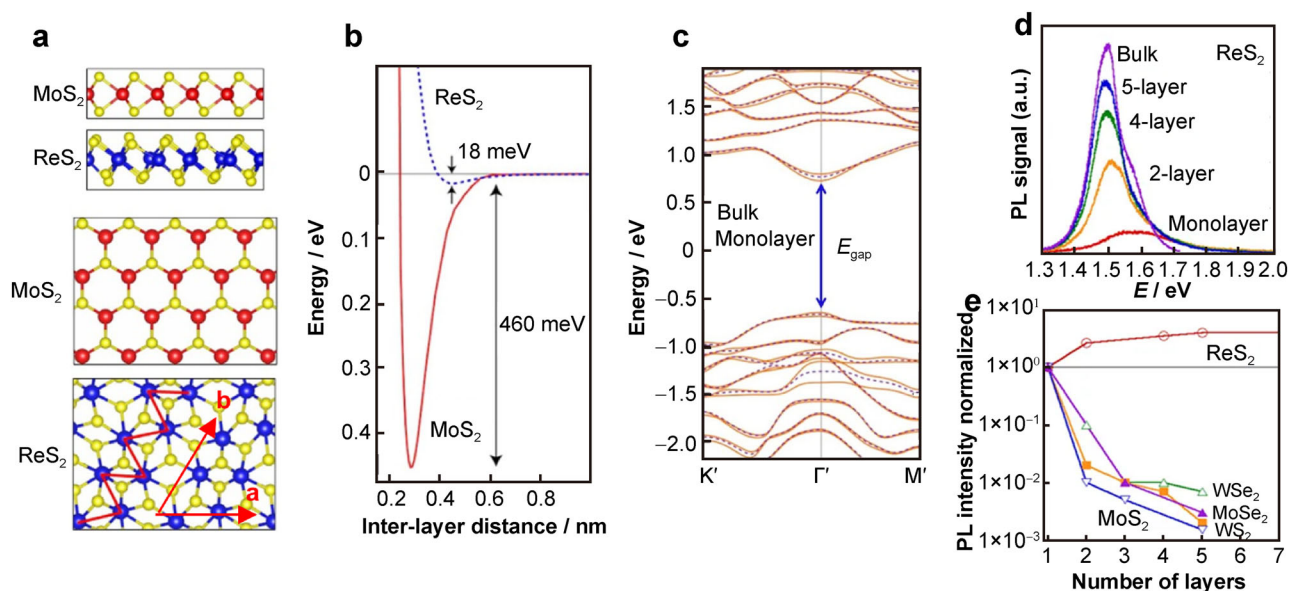
Fig. 3 Comparison of properties of ReS₂ with other isotropic TMDCs: **a** side and top views of crystal structures of 1H phase MoS₂ and 1T′ phase ReS₂; **b** weaker interlayer coupling energy in ReS₂ compared with MoS₂; **c** band structures of bulk (solid curves, E_{gap} = 1.35 eV) and monolayer ReS₂ (dashed curves, E_{gap} = 1.43 eV); **d** PL spectra of ReS₂ flakes with different thicknesses from bulk to a monolayer; **e** dependence of normalized PL intensity on layer number of ReS₂ and several types of isotropic TMDCs. Reprinted with permission from Ref. [26]. Copyright 2014 Nature Publishing Group, a division of Macmillan Publishers Limited

possesses seven valence electrons and one dangling electron [26, 36]. Because there are unbonded valence electrons outside the nucleus of Re, the four Re atoms in a unit cell will form a Re₄ cluster, which means that the Re–Re cluster forms a unique metal Re chain, reducing the structural symmetry. Therefore, a lattice distortion occurs on the basis of the 1T structure, and two crystal axes are formed after distortion. The Re-chain is denoted as the *b*-axis, and the direction with an angle of about 118.97° or 61.03° is denoted as the *a*-axis [27]. In addition, the extra electron in the Re atom greatly reduces the symmetry in layer and the van der Waals interaction interlayers. The low lattice symmetry and weak interlayer coupling result in ReS₂ possessing fascinating properties, especially in terms of the potential applications related to its anisotropic characteristics.

2.2 Optical properties

2.2.1 Band structure

The band structures of semiconductors determine their light absorption and luminescence properties. The band structures of layered TMDCs are mainly ascribed to the joint influence of the d-orbital electrons of the unbonded metal atoms and the p-orbital electrons of the chalcogenide atoms [37]. The bandgaps are usually dependent on the number of layers. In the case of MoS_2, when the bulk material reduces to a monolayer, it becomes a direct-bandgap semiconductor due to the quantum confinement effect and interlayer coupling [6, 38, 39]. In contrast to conventional TMDCs, in which the bandgaps are strongly dependent on the layer number, the band structure of ReS_2 changes only slightly with different thicknesses, which results from the weak interlayer coupling between the distorted lattices. According to density-functional theory (DFT) calculations, the interlayer coupling energy of ReS_2 is 18 meV, which is much weaker than that of MoS_2 (460 meV), as shown in Fig. 3b. The contributions from the d-orbital electrons of Re and p-orbital electrons of S lead to the valence and conduction band edges of ReS_2 [26]. The conduction band minimum (CBM) and the valence band maximum (VBM) coincide at the Γ point, resulting in direct bandgaps that are not related to the layer numbers [40], as shown in Fig. 3c. The bandgap energy changes from 1.35 to 1.43 eV when ReS_2 changes from the bulk material to a monolayer. Therefore, ReS_2 has a great potential for application in optoelectronic devices due to its optical transitions in the near-infrared region.

The direct recombination of electron–hole pairs dominates the recombination process in a semiconductor with direct bandgaps, which usually has a high quantum yield. Consequently, the PL intensity of monolayers is evidently higher than that of few layers or the bulk material of Mo- and W-dichalcogenides [26]. Owing to the interlayer coupling and quantum confinement, the PL intensity of Mo- and W-dichalcogenides decreases as the number of layers increases (Fig. 3e). Owing to the changes in the bandgap energy, the PL peak positions increase with a decrease in layer numbers [6]. In contrast, the PL intensity of ReS_2 is enhanced as the number of layers is increased (Fig. 3d, e). The PL peak positions of ReS_2, located between ~1.5 and 1.6 eV, do not move significantly when the material is thinned down to a monolayer (Fig. 3d), which verifies the weak interlayer coupling of ReS_2. Because the reduction of layer numbers does not enhance the quantum confinement of electrons in ReS_2, and the adjacent monolayers achieve electron decoupling [26], the PL peak position of ReS_2 is almost independent of the number of layers.

2.2.2 Optical anisotropy

In addition to the unique PL properties related to the band structure and the weak interlayer coupling of ReS_2, the triclinic lattice of ReS_2 with its reduced symmetry also generates the spatial anisotropic optical properties, such as optical absorption anisotropy and the polarization-dependent photoresponse [41, 42]. The anisotropic absorption coefficient and transient absorption coefficient reach a maximum when the light polarization is parallel to the Re-chain, while the minimum occurs when the light polarization is perpendicular to the Re-chain [43].

Low-symmetry lattices result in diverse light-matter interactions in ReS_2, such as changes in the amplitude and phase of light caused by the interaction with anisotropic materials. Angle-resolved polarized contrast spectroscopy can also reveal the optical anisotropy in ReS_2 flakes, which is a fast and non-destructive way to identify crystal axes [44]. A schematic configuration of the angle-resolved polarized optical contrast spectroscopy is shown in Fig. 4a. The spectra were obtained in a backscattering geometry using a white light source, and the ReS_2 on a SiO_2/Si substrate was rotated anticlockwise from 0° to 180° on a sample holder. θ is the included angle between the polarization of the incident light and the direction of the Re–Re chains (b-axis). Figure 4b shows the polarized optical contrast spectra of monolayer ReS_2 at different angles. The peak contrast at about 608.0 nm decreased as θ increased from 0° to 90°, which means that the contrast was maximum when the light polarization was parallel to the Re-chain. The change of contrast intensity at 608.0 nm in Fig. 4c reveals a periodical variation with different included angles, and the maximum and minimum intensities occurred at 0° and 90°, respectively. The higher contrast intensity indicates a stronger photon-matter interaction along the direction of the Re–Re chains ($\theta = 0°$). Owing to the difference in the complex refractive index in the direction of the Re–Re chains and that perpendicular to the Re–Re chains, the reflectivity will be different in the amplitude and phase shift, resulting in polarized light. Therefore, the amplitude and phase anisotropy of the reflected light are dependent on the direction of the Re–Re chains.

Raman spectroscopy is a nondestructive and fast detection technique that can reveal the optical properties related to anisotropy. It has been extensively used to identify the layer number, stacking order, and interlayer coupling of 2D materials [45]. The shear modes and breathing modes at low frequencies (< 50 cm^{-1}) indicate the relative vibration between different layers, as determined by the van der Waals interaction [46–48]. The weak interlayer coupling energy in ReS_2 results in decoupled lattice vibrations between adjacent layers, with the result
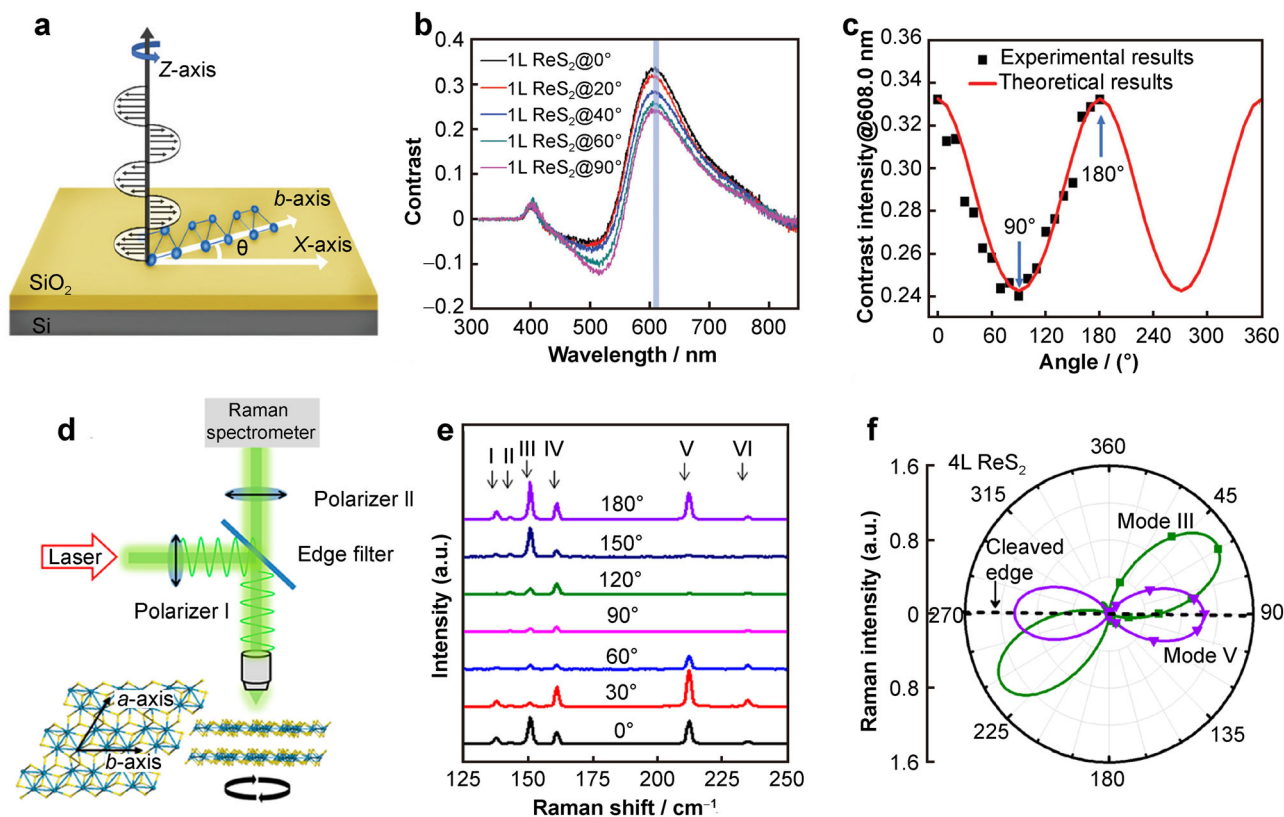
Fig. 4 Anisotropic optical properties of ReS₂: **a** schematic illustration of a polarized light contrast spectroscopy analysis; **b** polarized optical contrast spectra of 1L ReS₂ at included angles of θ = 0°, 20°, 40°, 60° and 90°, where contrasts at 608.0 nm are highlighted by a light blue bar; **c** contrast intensities of 1L ReS₂ at 608.0 nm at different included angles. Reprinted with permission from Ref. [44]. Copyright Clearance Center, Inc. **d** Configuration of angle-resolved polarization Raman measurement and (inset) top view of crystal structure of ReS₂; **e** Raman spectra of ReS₂ at different rotation angles under a laser of 514.5 nm. Reprinted with permission from Ref. [58]. Copyright 2017 American Chemical Society. **f** Angle-resolved Raman intensities for mode III and V of 4L ReS₂ shown in a polar plot. Reprinted with permission from Ref. [59]. Copyright 2015 American Chemical Society

that ReS₂ exhibits a few complex Raman modes [26, 46]. Owing to the low crystal symmetry of ReS₂, the shear modes of bilayer ReS₂ are not degenerate and can be divided into parallel vibration ($S_1^\parallel$) and perpendicular vibration ($S_1^\perp$) relative to the Re chain [49]. The two shear modes (13.0 and 16.5 cm⁻¹) can be distinguished in contrast to the vibrations of TMDCs with isotropic structures [50–52]. In the high-frequency range of 100–450 cm⁻¹, there are 18 Raman vibration modes of ReS₂, including six in-plane vibration modes, four out-of-plane vibration modes, and eight coupled modes. These high-frequency modes reveal the relative atomic vibration in-plane, which is determined by the chemical bond interactions connecting the in-plane atoms. The differences in the Raman spectra of the bulk and monolayer ReS₂ are negligible [35]. The tensor form of a Raman-active phonon mode relies on the symmetry of both the crystal and lattice vibration [53]. There are off-diagonal elements in the polarizability tensor for anisotropic crystals. Therefore, the intensity of the Raman-active modes in anisotropic 2D layered materials is

polarization-dependent and changes periodically with the polarization angles due to the reduced in-plane symmetry [54–57]. Figure 4d shows a schematic configuration of the angle-resolved polarization Raman measurement with the excitation of polarized laser and rotation of the sample in-plane [58]. The Raman spectra of the exfoliated ReS₂ flake at different rotation angles are shown in Fig. 4e. The Raman intensities of all the vibration modes vary periodically with the rotation angle at a period of 180°, which indicates the anisotropic optical characteristics of ReS₂. According to the DFT calculations, Mode III at ∼ 150 cm⁻¹ is mainly composed of the in-plane vibrations, and Mode V at ∼ 211 cm⁻¹ contains both the out-of-plane vibrations of sulfur atoms and the in-plane vibrations of Re atoms in the b-axis direction [26, 59]. Figure 4f shows a polar plot of the Raman intensity for Modes III and V in 4L ReS₂. The maximum intensity of Mode III appears at an angle of ∼ 58°, while the maximum intensity of Mode V occurs at an angle of ∼ 91°, which corresponds to the cleaved edge of the exfoliated

flake. As a result, the Raman intensity of Mode V is usually utilized to determine the crystal direction of the b-axis in ReS$_2$ flakes [44]. Therefore, ReS$_2$ shows strong in-plane polarization in Raman scattering, and the crystal orientation can be determined according to Raman spectra.

2.3 Anisotropic thermal conductivity

Thermal conductivity is a fundamental property of materials and reflects the atomic bonding strength and crystal symmetry. In integrated small-scale devices, power consumption and heat conduction are crucial for the performance of the chip. It is, therefore, vitally important to understand the thermal transport properties of ReS$_2$, especially considering its potential applications in FETs and photodetectors. As an anisotropic material, the differences in phonon coupling caused by lattice vibration in the different orientations of ReS$_2$ will inevitably lead to anisotropic thermal conduction.

The thermal conductivity of single-crystalline ReS$_2$ has been measured at room temperature using time-domain thermoreflectance (TDTR) [60], where the pump laser beam is modulated by an electro-optic modulator, creating temperature excursions in the samples. The probe laser beam interrogates the temperature changes at the sample surface. Mechanically exfoliated ReS$_2$ flakes were mounted on a rotation stage, and the Re-chain direction of the flakes was oriented along either the horizontal (X) or vertical (Y) directions, which is determined by polarized Raman measurements. A thin film of Nb$_{0.43}$V$_{0.57}$ alloy with about 70 nm in thickness was deposited on the samples prior to the measurements to serve as an optical transducer. Figure 5a shows the TDTR signals collected as a function of the beam-offset, where the intensity profile of the laser beam is represented by the dashed curves. Under the low modulation frequency of 1.1 MHz, the TDTR signal followed the Gaussian profiles of the laser beam intensity,

while the lateral heat spreading in the sample was slightly larger than the beam size. Figure 5b is a 2D scan of the TDTR signal for the flake in Fig. 5a and shows that the Re-chains were oriented along the horizontal axis (X). The TDTR signal was wider along X (i.e., the full width at half maximum (FWHM) of V_{out} was 6.32 μm (X) and 6.18 μm (Y)), implying that the thermal conductivity was larger in the direction parallel to the Re-chains. In addition, for different sample thicknesses, the derived in-plane thermal conductivity of ReS$_2$ also displayed an orientation dependence, as shown in Fig. 5c. The in-plane thermal conductivity was higher along the parallel direction of Re-chains (70 ± 18) W·m^{-1}·K^{-1} than in the perpendicular direction (50 ± 13) W·m^{-1}·K^{-1}. Moreover, the orientation-dependent in-plane thermal conductivity of ReS$_2$ was higher than the through-plane thermal conductivity (0.55 ± 0.07) W·m^{-1}·K^{-1}, indicating a notably high anisotropy of the in-plane to the through-plane thermal conductivity. The anisotropic in-plane thermal conductivity together with the interface thermal conductance between the ReS$_2$/electrode and ReS$_2$/substrate, will be helpful for the new approach of exploring nanoscale devices based on anisotropic 2D materials.

3 Synthesis methods

Large-scale and high-quality production of 2D layered TMDCs is crucial for fundamental research and practical applications. Generally, the "top-down" and "bottom-up" methods are used to prepare monolayer or multilayer 2D materials. Rhenium disulfide has a unique distorted lattice and high in-plane anisotropy. The high-quality and large single crystal of ReS$_2$ is essential for the preparation of monolayer or multilayer ReS$_2$ by mechanical exfoliation. A modified Bridgman method was utilized to grow single crystal of ReS$_2$ with a thickness of hundreds of
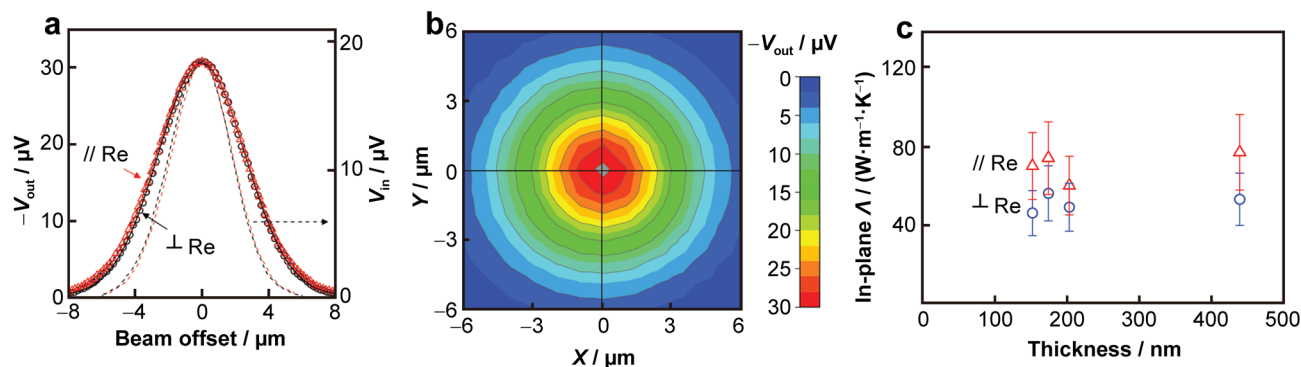
Fig. 5 **a** In-plane TDTR data for a ReS$_2$ flake at a modulation frequency of 1.1 MHz and time delay of −50 ps; **b** 2D beam-offset scan of TDTR signal; **c** in-plane thermal conductivity (∧) of ReS$_2$ flakes as a function of thickness. Reprinted with permission from Ref. [60]. Copyright 2017 WILEY–VCH Verlag GmbH & Co. KGaA, Weinheim

micrometers, which can avoid the unintended doping caused by using a halogen transport agent [61]. The controllable anisotropic growth of ReS$_2$ thin film requires deep understanding on the growth mechanism of grains. Lots of preparation methods have been used to obtain high-quality ReS$_2$ thin layer to apply in the devices.

3.1 "Top-down" method

One typical synthesis method for ReS$_2$ is mechanical or chemical exfoliation according to the "top-down" strategy. Mechanical exfoliation, i.e., peeling the flakes from the surface of a ReS$_2$ crystal with tape, can provide samples with good crystalline quality and few defects. Therefore, it is widely used in the study of intrinsic physical properties and for the preparation of high-performance devices [62]. However, mechanical exfoliation cannot realize large-scale fabrication, which is essential in industrial applications. An attempt to solve this problem has been made by employing chemical exfoliation or liquid exfoliation [62, 63]. One such liquid exfoliation method is to intercalate specific metal ions (mainly lithium ions) between layers, which increases the interlayer spacing, weakens the interaction between layers, and reduces the energy barrier of stripping, so achieving exfoliation. However, the intercalation of lithium ions can negatively charge the exfoliated nanosheets, even inducing a phase transition in 2D layered TMDCs [62, 64]. Sonication-assisted liquid exfoliation is another type of large-scale liquid exfoliation method. 2D layered materials can be obtained in a specific solvent by the ultrasonic cavitation effect. The matching of the surface energy of the layered crystal and the solvent is crucial for efficient exfoliation [65]. Therefore, it is important to find a suitable solvent for the exfoliation of bulk ReS$_2$. By selecting the solvent and controlling the sonication time, temperature, or power, the controllable fabrication of nanosheets can be obtained with a tunable concentration, size, and thickness. Although sonication-assisted liquid exfoliation can realize the cost-effective and high-yield production of 2D nanosheets in a simple process, the lateral size of the nanosheets is relatively small, and there are usually many defects or impurities.

3.2 "Bottom-up" method

3.2.1 Physical/chemical vapor deposition

The "bottom-up" strategy, including physical vapor deposition (PVD) and chemical vapor deposition (CVD), can be employed to produce large-scale 2D materials with high purity. Physical vapor deposition refers to physical processes, such as the thermal evaporation of materials, in which the atoms, molecules, or partially ionized ions can be evaporated from the surface of precursors when they are heated or bombarded, and form thin films on a substrate. The reported PVD-prepared ReS$_2$ films are polycrystalline, with different grain orientations. The size of the sample is relatively large, but the thickness is difficult to control at the atomic level [66]. Using the CVD method with tunable growth parameters, the quality and uniformity of the synthesized films can be improved, which has been proven to be an effective way to ensure the large-scale controllable production of 2D materials. The lateral size, layer number, and morphology of a monolayer or few-layer crystals can be adjusted by the type of precursor or substrate, the saturated vapor pressure, growth temperature, and the flow rate of the carrier gas.

Figure 6a is a schematic illustration of the CVD synthesis of ReS$_2$. The solid precursors of Re and S are heated to the vapor phase and then react on the substrate to form large monolayer crystals. The large-scale anisotropic growth of ReS$_2$ is realized by controlling the growth parameters. After selecting specific precursors, the growth time can be controlled to adjust the morphology of ReS$_2$. For example, using rhenium powder and sulfur powder as precursors, thick hexagonal ReS$_2$ flakes have successfully been fabricated on the substrate, whereas they were not stable in heating process [67]. With an increase in growth time, some of the flakes became thinner or even disappeared, leaving only the triangle frameworks, and finally, ReS$_2$ nanoribbons were obtained. The reaction temperature has a great influence on the morphology of the synthesized ReS$_2$ samples [68]. As shown in Fig. 6b–e, the morphology of ReS$_2$ varies at different temperatures, from a circle at 500 °C to a hexagon at 600 °C, then to a serrated structure at 700 °C, and finally to a dendritic structure at 850 °C [69]. At low temperatures, due to the slow diffusion of atoms and the unfree attachment and detachment of adatoms at the edges, the epitaxial growth along different crystal axes occurs at almost the same rate (Fig. 6b). At higher temperatures, the diffusion of atoms is rapid, and the adatoms tend to migrate and attach to the high-activation growth direction [010]. Therefore, at higher growth temperatures, the asymmetric growth of ReS$_2$ becomes evident (Fig. 6e). Furthermore, the type of substrate also affects the film size. With glass as the substrate and ReO$_3$ powder as the precursor, the continuous fabrication of uniform wafer-scale ReS$_2$ multilayers (7 cm × 2 cm) has been achieved [70]. Using mica as the substrate, both the mass of the sulfur source and flow rate of the carrier gas have been shown to affect the nucleation density of ReS$_2$, and thus the film size. A high-quality monolayer film, with a size of about 2 mm, can be obtained using this method [71].

Recent studies on the CVD growth of ReS$_2$ have focused on the improvement of growth efficiency and the clarification of the growth mechanism. A tellurium-assisted CVD method was developed to use Re-Te binary eutectic
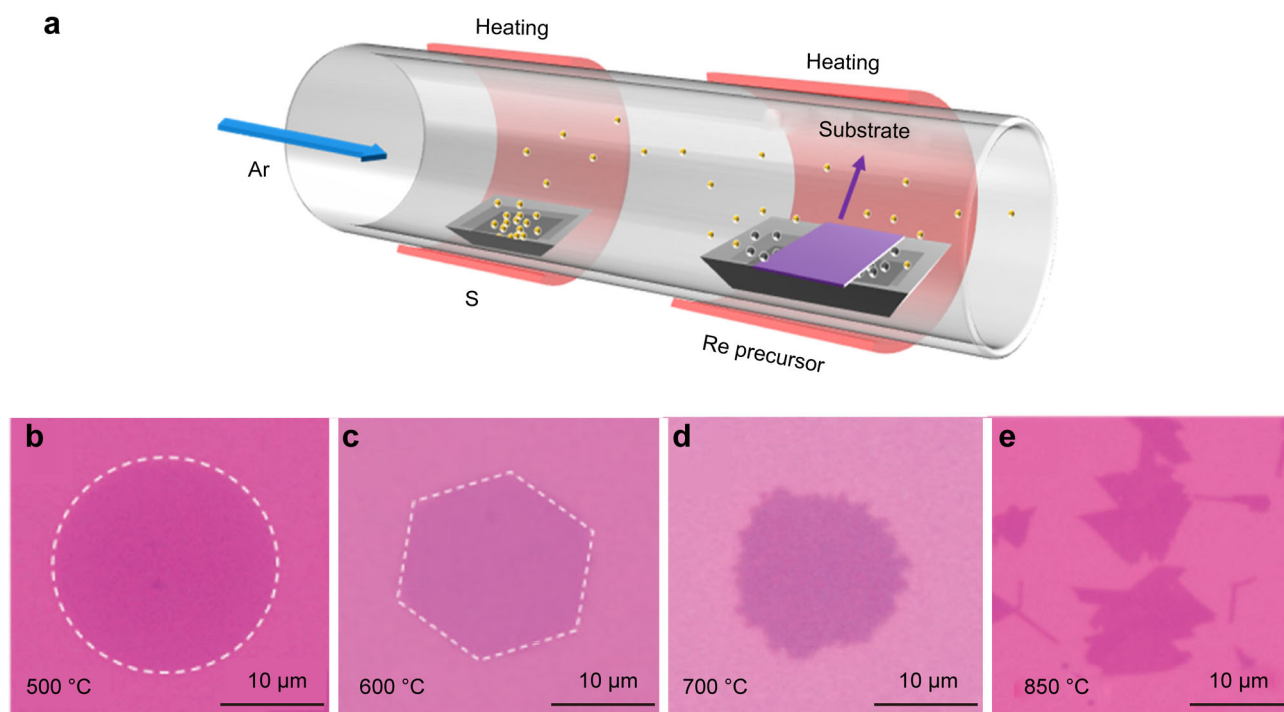
Fig. 6 **a** Schematic illustration of CVD synthesis of ReS₂, where yellow ball represents sulfur atom and gray ball represents rhenium atom; **b-e** optical images of monolayer ReS₂ products grown at different temperatures and transferred onto SiO₂/Si substrates. Reprinted with permission from Ref. [69]. Copyright 2016 WILEY–VCH Verlag GmbH & Co. KGaA, Weinheim

as the Re source, which effectively reduced the melting point of Re and increased the vapor pressure of ReS₂ in the reaction system, thus increasing the growth efficiency [69]. To investigate the growth mechanism, the microstructure of the fabricated ReS₂ flakes was characterized by angle-resolved polarized optical microscopy, which showed that the monolayer flakes are composed of subdomains, with different types of grain boundaries (GBs) between them [72]. The formation of the domain structures and the limitation of domain size were explained by a dislocation-involved anisotropic evolution mechanism [71]. Because the interface energy could affect the domain size of ReS₂, increasing the growth temperature would be beneficial to increase the domain size [71]. When the growth temperature was increased to 700 °C, the single-crystal ReS₂ domains tended to grow into triangles, with a lateral size of 30–40 μm. Based on the understanding of the growth mechanism and the precise control of the grain orientations and boundary splicing, the large-scale production of single crystal ReS₂ can therefore be obtained, and is likely to be useful in device applications.

3.2.2 Hydro-/solvothermal synthesis

Another representative "bottom-up" method is wet-chemical synthesis, which relies on the chemical reactions of precursors in solution under proper conditions. The wet-chemistry method has been widely used to synthesize ultrathin 2D nanomaterials due to the high production yield of the synthetic materials. As a typical wet-chemistry method, hydro-/solvothermal synthesis uses water or organic solvent as the reaction medium in a sealed vessel. A high-temperature and high-pressure reaction environment can be created by heating the vessel, which is helpful to improve the crystallinity of the synthesized materials. In recent years, the hydro-/solvothermal synthesis of ReS₂ has been widely utilized [73–76]. A one-pot hydrothermal method was used to prepare porous composites of ReS₂/CNTs, where ReS₂ nanosheets directly nucleated on the walls of CNTs [73]. The special capacity of ReS₂/CNTs composites was larger than the theoretical capacity of bulk ReS₂ (430 mAh·g⁻¹), and the electrochemical performance was significantly improved compared with that of pure ReS₂ [77]. In addition, few-layered ReS₂ nanosheets were prepared by the direct nucleation on reduced graphite oxide (RGO) through a hydrothermal method [74]. The highly conductive and porous networks of RGO facilitate the electrolyte infiltration and the charge transfer [74, 78, 79]. The ReS₂/RGO composites had good electrocatalytic performance because of more electrochemical active sites from ReS₂. Although hydro-/solvothermal method has high production yield and is cost-effective, the reaction is

difficult to precisely control, because it usually involves simultaneous multi-step reactions at high temperature and pressure. The temperature, pressure, reaction time, precursor concentration, and other factors affect the type and morphology of the product, so it is difficult to predict the structure of synthetic materials. Consequently, it is more suitable to prepare large-scale multilayer samples, instead of monolayers, for the electrochemical or catalytic applications.

4 Applications

With the integration and miniaturization of FET devices in Si-based technology, it has become a great challenge to further reduce the device size. When the channel length of a FET is reduced to several nanometers, the threshold voltage decreases and the leakage current is dramatically increased. The reduction of gate modulation then leads to an increase in sub-threshold swing. To solve the short channel effect, 2D semiconductors, with ultrathin thicknesses and unique physical properties, are promising candidates as channel materials for post-silicon electronics.

Most TMDCs are isotropic materials and have been widely studied in device development. However, reducing the lattice symmetry of TMDCs can induce interesting physical properties. Anisotropic electrical transport, magnetic, photoelectric, piezoelectric, and ferroelectric properties of low symmetry 2D TMDCs have been reported [13]. The study of these anisotropic materials can provide new ways to modulate their properties and the possibility of optimizing device performances. The unique crystal structure and strong in-plane anisotropy of ReS₂ have resulted in the widely utilization in the research and development of functional devices, including optoelectronics, logic, electrocatalysis, and energy storage [62]. In the following section, the application of its anisotropic characteristics, such as its electrical transport, photoelectric, and logic properties, is reviewed. Devices based on the van der Waals heterostructures (vdWHs) of ReS₂ are then introduced.

4.1 Anisotropic devices of ReS₂

#### 4.1.1 Anisotropic FETs and logic devices

Many FET or logic devices based on 2D semiconductors have been demonstrated by combining two different 2D transistors, e.g., n-type and p-type. However, in the future, integrated devices based on anisotropic 2D semiconductors can be designed and adjusted using lattice orientation as a variable [27].

The relationship between the lattice orientation and the carrier mobility has been studied in FETs based on ReS₂. As shown in Fig. 7a, the electron mobilities are closely related to the crystal orientation angles. The direction with the minimum mobility (μ_{min}) at 0° or 180° was set as the reference. It was found that the direction with the maximum mobility (μ_{max}) occurred at 120° (or 300°). The detected anisotropic ratio of mobility (μ_{max}/μ_{min}) was 3.1. Moreover, two FETs fabricated on the same flake of ReS₂ could form an integrated digital inverter, as shown in Fig. 7b. The channel of the left FET is along the a-axis and that of the right FET is along the b-axis, where the Re-chain is indicated by the red ribbon. A circuit diagram and an optical image of the digital inverter are shown in Fig. 7c. The top gate voltage on the a-axis is fixed to be -2 V, while that on the b-axis is the input voltage (V_{in}), and the shared electrode in the middle is the output voltage (V_{out}). Studies of the digital inverter device integrated by two ReS₂ FETs have not only provided a new method to design logical devices by utilizing the lattice anisotropy, but also shown that the unique properties of low symmetry 2D semiconductors can be exploited to develop new applications in future.

4.1.2 Anisotropic optoelectronic devices

Optoelectronic devices based on 2D TMDCs have been widely studied due to their tunable bandgap, flexibility, and dangling-bond free structure, which have provided useful information regarding the light detection and imaging of post-silicon devices. Intense efforts have been made to develop optoelectronic devices that have the advantages of a short response time, high efficiency, high photosensitivity, and wide response frequency [80]. Among the different types of devices based on TMDCs, the optoelectronic devices made from anisotropic TMDCs have gradually attracted increasing attention due to the efficient polarization detection in experimental studies [81–83].

As one of the typical anisotropic TMDCs, ReS₂ has the potential for a wide range of applications in optoelectronic devices because of its novel electronic performance and polarization-related characteristics. The existence of a direct bandgap, independent of layer numbers, enables it to not only process a high absorption coefficient under photoexcitation, but to also produce efficient electron–hole pairs, which are the key factors in high-performance photodetectors [81]. Figure 8a shows a polarization-sensitive photodetector based on the anisotropic structure of ReS₂ [81]. When the energy of an incident photon is larger than the bandgap of a semiconductor, the photogenerated electron–hole pairs are laterally separated by applying a drain bias voltage, resulting in a photocurrent. Figure 8b shows
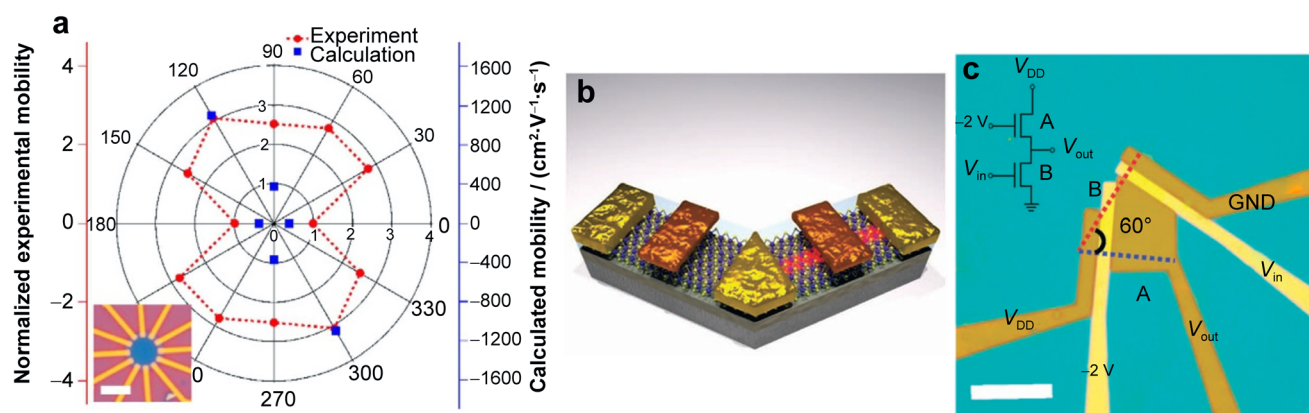
Fig. 7 **a** Normalized field-effect mobility of a six-layer ReS$_2$ device along 12 directions; **b** schematic illustration of a digital inverter based on two ReS$_2$ FETs, where Re-chain is indicated by red ribbon; **c** optical image of a ReS$_2$ digital inverter and (inset) circuit diagram. Reprinted with permission from Ref. [27]. Copyright 2015 Natural Publishing Group
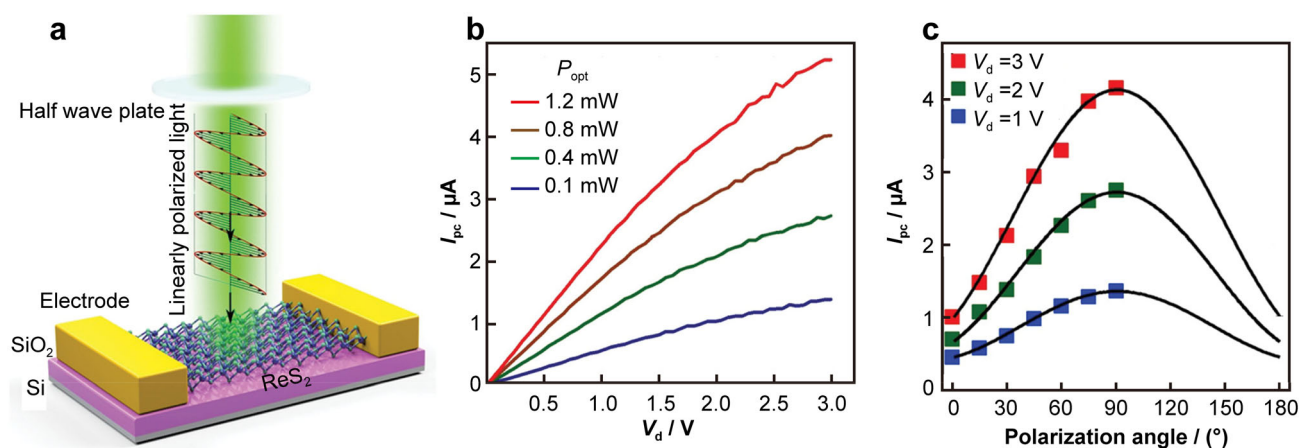
Fig. 8 **a** Schematic of ReS$_2$ photodetector, illuminated by a linearly polarized green light (2.4 eV); **b** photocurrent as a function of drain voltage under different incident powers; **c** photocurrent as a function of the polarization angle under different drain bias voltages, where a power law function was found to fit data well (black line). Reprinted with permission from Ref. [81]. Copyright 2016 WILEY–VCH Verlag GmbH & Co. KGaA, Weinheim

that the photocurrent (I_{pc}) increases with the drain bias (V_d) increasing under different light powers. The photocurrent can be significantly changed by rotating the polarization of light at the same incident power. The photocurrent as a function of the polarization angle of the incident light is shown in Fig. 8c, where the drain bias voltage (V_d) is 1, 2 and 3 V, respectively. Under different drain bias voltages, when the polarization angle reaches 90°, corresponding to the direction of the Re$_4$ chain in ReS$_2$, the photocurrent reaches its maximum value. Owing to the different optical absorption properties of ReS$_2$ in-plane, the polarized photocurrent along the *b*-axis is much stronger than that perpendicular to the *b*-axis. This discovery proved that atomic thin ReS$_2$ can be used in light polarization detection and practical integrated optical applications.

4.2 Devices based on vdWHs

The development of an atomically thin semiconductor heterojunction is one way to solve the limitation of traditional semiconductors caused by the short channel effect. Ultrathin 2D heterostructures can be assembled by two different kinds of 2D materials with the weak van der Waals interaction between them forming perfect interfaces, which are usually termed as vdWHs. In contrast to the epitaxial growth of thin films of traditional semiconductors, the fabrication of vdWHs does not involve lattice matching. They can be prepared by precisely stacking different 2D materials, with a rational design. In recent years, vdWHs based on TMDCs have been widely studied in switching devices, electronic and optoelectronic devices,

semiconductor lasers, solar cells, and logic devices [84–87]. Because the 2D TMDCs containing in the vdWHs have different bandgaps, a wider spectral response can be achieved than homojunctions. Furthermore, reducing the in-plane symmetry in 2D ultrathin TMDCs can induce the anisotropic properties of electro-optical responses. The development of ultrathin vdWHs consisting of in-plane anisotropic 2D materials is therefore of great significance for studying the effect of asymmetric lattices on physical properties.

4.2.1 Optoelectronic heterostructure devices

Most TMDCs possess tunable bandgaps in the range of 1–2 eV [5–8], which are usually dependent on the number of layers. When the thickness is reduced to a monolayer, TMDCs usually show direct bandgaps, indicating a high light responsivity, but low light absorption. With the weak interlayer coupling and a direct bandgap independent of the layer number, the few-layer ReS₂ has a high density of edge states and enhanced light absorption, which provides a good platform for studying optoelectronic devices built by vdWHs. To overcome the low light absorption of the monolayer, a mixed-thickness ReS₂/Si heterostructure (Fig. 9a) was prepared with a high optical responsivity ($\sim$33.5 A·W^{-1}) and fast response time (80 μs). It provided a new method to solve the trade-off between the responsivity and response time in the multilayer TMDC heterostructure [88]. In addition to increasing light absorption using a multilayer ReS₂, the interface edge state provides a strong possibility of charge scattering (acting as carrier trapping sites) and therefore plays an important role in the enhancement of the responsivity and response time. The photogenerated holes are separated and transferred to Si through the valence bands of multilayer ReS₂, while the photogenerated electrons drift toward the electrodes and are partially trapped in the bulk defect states of ReS₂ and the edge states at the interface of mixed-thick ReS₂. The photocurrent and external quantum efficiency (EQE) under 532-nm-laser irradiation are shown in Fig. 9b, c, respectively. Among the devices fabricated by different thicknesses of ReS₂, the mixed-thickness ReS₂/Si heterostructures had the highest EQE value and the fastest response speed. Therefore, at the mixed thickness ReS₂/Si heterointerface, the gain associated with the photogenerated carrier trapping is dominant at the ReS₂ interface between different layers, which also results in a high photoresponsivity.

To improve their optoelectronic performances, TMDCs and other low-dimensional materials can be combined to build heterostructures due to their promising semiconducting electrical properties. A photodetector based on a ReS₂/graphene heterojunction was prepared with ReS₂ as the optical absorption layer and graphene as the transport layer [89]. The photoresponsivity was 7×10^5 A·W^{-1}, the detectivity was 1.9×10^{13} Jones, and the response time was less than 30 ms due to the synergistic effects between graphene and ReS₂. Because of the high carrier mobility in graphene, the transport rates of the photogenerated carriers in ReS₂ were enhanced. Compared with monolayer ReS₂, the photon energy absorption per unit area of the multilayer was increased due to the thickness and long light path, which also enhanced the photocurrent and responsivity. This discovery has helped to develop optoelectronic devices with high sensitivity and fast response, such as heartbeat sensors or optical communication devices. Black phosphorus is considered to be a candidate material to replace graphene and has great potential in ultrafast optoelectronic applications due to its tunable direct bandgap and unique 2D anisotropic structure. As shown in Fig. 9d, a vdWH with gate-tunable rectifying behavior was made from an exfoliated n-type multilayer ReS₂ and p-type BP [90]. The current rectification characteristics of the device were modulated by adjusting the back-gate voltage (Fig. 9e). With an increase in the positive gate voltage, the rectification ratio increased. When the channel length was 1.6 μm for ReS₂ and 4 μm for BP, the heterojunction exhibited a responsivity of 4120 A·W^{-1} without gating under a UV light ($\lambda = 365$ nm). By changing the BP channel length to 1 μm, a higher photoresponsivity of 11,811 A·W^{-1} was achieved at the back-gate voltage of 4.4 V, as shown in Fig. 9f.

The development of ultrathin heterojunctions consisting of in-plane anisotropic TMDCs and isotropic TMDCs is critical in determining the effect of asymmetric lattices on their physical properties. The interlayer coupling between the anisotropic/isotropic interfaces in a ReS₂/MoS₂ heterojunction has been characterized by in situ Raman spectroscopy, electrical, and photoelectrical measurements [91]. After interfacing with monolayer ReS₂, the in-plane vibrational mode of MoS₂ was softened and the out-of-plane vibration mode was stiffened, which highlights the interlayer coupling in the heterostructure. This device exhibited a current rectification and prominent gate-modulated transport characteristics. Under the excitation of a 532-nm laser, the ReS₂/MoS₂ heterojunction produced an optical response with a responsivity of $\sim$ 35 A·W^{-1} at a bias voltage of 2 V without gating. Additionally, a monolayer 1T' ReS₂-ReSe₂ lateral p–n junction (Fig. 9g) was prepared through a two-step epitaxial growth method [92]. Figure 9h shows the transfer curves of the individual ReSe₂ and ReS₂ domain in the FETs, revealing typical n-type and p-type conduction characteristics, indicating that the individual ReS₂ and ReSe₂ domains were of high quality and might form p–n junctions. As shown in Fig. 9i, the lateral ReS₂-ReSe₂ heterojunction exhibited a good rectification,
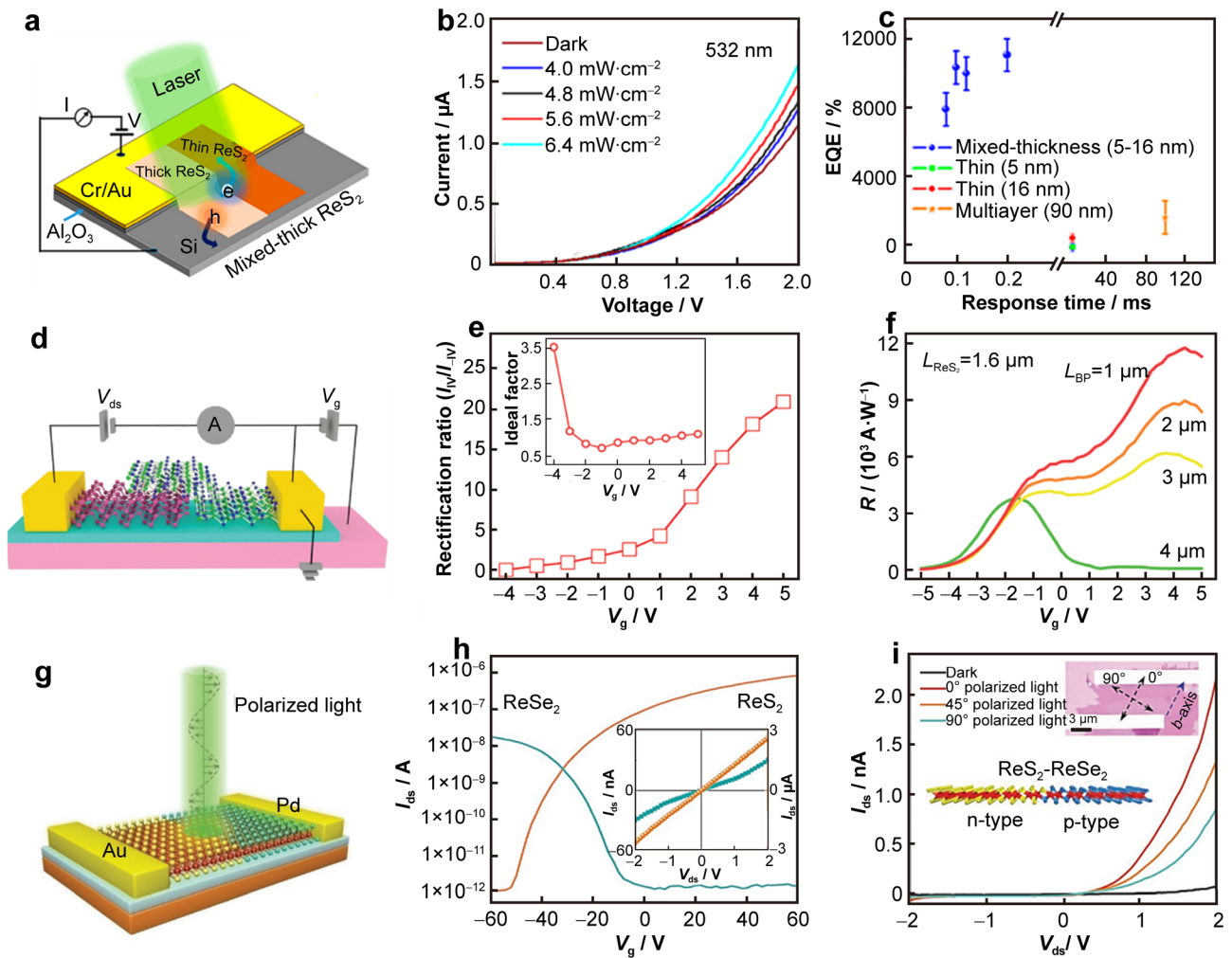
Fig. 9 **a** Schematic illustration of a mixed-thickness ReS₂/Si heterojunction; **b** I_{ds}–V_{ds} curves of mixed-thickness ReS₂/Si heterojunction in dark and under different incident power densities; **c** comparison of the EQE values of four different ReS₂/Si photodiode structures under a 532-nm-laser irradiation. Reprinted with permission from Ref. [88]. Copyright 2019 American Chemical Society. **d** Schematic illustration of vertical BP/ReS₂ heterojunction device; **e** current rectification ratio as a function of back-gate voltage (V_g) and (inset) diode ideal factor as a function of V_g under a forward bias (factor of 1.0 indicates a good interface quality in BP/ReS₂ heterojunction); **f** photoresponsivity as a function of back-gate voltage with increased L_{BP} values under an illuminated power density of 0.55 mW·cm⁻². Reprinted with permission from Ref. [90]. Copyright Clearance Center, Inc. **g** Schematic of lateral ReS₂/ReSe₂ heterojunction device using linearly polarized light as excitation source; **h** transfer curves (I_{ds}–V_g) of individual ReSe₂ and ReS₂ domain in FETs and (inset) I_{ds}–V_{ds} curves for individual ReSe₂ and ReS₂ domain; **i** transport curves (I_{ds}–V_{ds}) of ReS₂/ReSe₂ heterojunction device with various polarization angles (λ = 532 nm; power: 50 nW), where light polarization directions relative to b-axis of heterojunction (as indicated by blue dashed arrow in inset) are 0°, 45° and 90°, respectively, and inset shows an optical image of heterojunction device. Reprinted with permission from Ref. [92]. Copyright 2018 WILEY–VCH Verlag GmbH & Co. KGaA, Weinheim

with a threshold voltage of 0.6 V under a forward bias. Moreover, the photocurrent (I_{ds}) was dependent on the polarization direction of the incident light. When it is parallel to the lattice direction of the heterostructure (b-axis), I_{ds} was much larger than that when the direction was perpendicular to the b-axis of the heterojunction. These results not only showed the fundamental characteristics of photodiode dependent on the light polarization, but also realized the linear dichroism in the 2D lateral heterostructure, which is likely to be of great significance in the development of new devices with multiple functions.

4.2.2 Logic devices based on 2D heterojunctions

With the continuous developments in the use of big data, the requirements for the speed and efficiency of computer operation are gradually increasing. Breaking the traditional von Neumann computer architecture is one way to develop new logical operating devices. Negative differential resistance (NDR) devices have many threshold voltages and play an important role in the application of multivalued logic. Owing to the diversity of band structures, 2D van der Waals heterojunctions have great

potential in multi-functional devices, including memory and logic devices.

In the realization of NDR devices, vdWHs composed of the dangling-bond-free 2D materials have been adopted to pursue an ideal peak-to-valley current ratio (PVCR) at room temperature [93–95]. In MoS_2/WSe_2 and BP/$SnSe_2$ devices, the band-to-band tunneling of carriers can be obtained, but with a relatively low PVCR. The type-II MoS_2/WSe_2 heterojunction needs a complicated fabrication process to obtain an electrostatically doped n^+/p^+ heterojunction. Using the type-III heterojunction with a broken-gap band alignment, it is easy to implement a highly doped n^+/p^+ heterojunction without an electrostatic or chemical doping process. For example, a BP/ReS_2 heterojunction with a broken-gap band arrangement was used to fabricate a NDR device [96]. The carrier transport mechanism of this NDR device was studied by considering the tunneling and diffusion currents. When a negative voltage (< 0 V) was applied, electrons tunneled from the BP filled valence band states to the ReS_2 empty conduction band states, thereby increasing the current. By applying a small positive voltage ($0 < V < 0.4$ V), the current also increased due to the tunneling of electrons in the conduction band states of ReS_2 to the empty valence band states of BP. If the Fermi level of ReS_2 coincides with the top of the valence band of BP, the filled states in ReS_2 overlap maximally with the unoccupied states in BP, thus leading to the maximum tunneling current. By further increasing the voltage ($0.4 < V < 0.9$ V), the current decreased because the bandgap reduced the overlap between the filled and empty states. Furthermore, when a higher voltage ($V > 0.9$ V) was applied, the tunneling current was no longer a factor influencing the operation of NDR device. Owing to the shrunken potential hill in the heterojunction, the electron carriers in ReS_2 can diffuse to BP, thus increasing the current. The carrier transport mechanism was studied by analyzing the tunneling and diffusion current at different temperatures, and an analytical model of the NDR device was established, which is essential for the application of 2D TMDCs in logical operations.

Nonvolatile logic devices can compute and store data in the same device, which will lead to benefits in terms of energy efficiency. Compared with traditional binary logic devices, multi-valued logic devices can achieve a higher data density with less disk space. A 2D van der Waals heterojunction based on BP and ReS_2 was made for non-volatile ternary logic operation, in which the thin phosphorus oxide (PO_x) layer from the natural oxidation of BP was used as both the charge trapping layer and the tunneling layer [97]. Using the FETs based on BP/ReS_2 heterojunctions and BP in series, a ternary logic circuit can be built. The logical states 1, 1/2 and 0 can be modulated by an input voltage pulse, resulting in a nonconventional logical output. Moreover, using handwritten digital data, an artificial neural network simulation based on electronic synapse arrays can obtain a high recognition accuracy of 91.3%. This provides a way to implement multifunctional non-volatile logical storage applications based on novel 2D heterojunctions.

4.3 Energy storage devices

4.3.1 Conductive electrode in alkali ion battery

With the rapid development of hybrid electric vehicles and electronics, novel energy storage technology has become an urgent field. Alkali (Li, Na, K) ion battery is widely explored because of their advantages of long cycle-life, fast charge–discharge capability, and environmental friendliness. Conductive electrode is one of the most important components in batteries; it usually restricts the performance of batteries. The large interlayer spacing (0.614 nm) and the weak interlayer interaction of ReS_2 facilitate the diffusion of alkali metal ions within layers, which enables ReS_2 as a candidate anode material for alkali ion batteries [98]. However, the anode prepared from pure ReS_2 has relatively low conductivity and poor cycle stability. Therefore, specific composites need to be designed to overcome the shortcomings and improve the performance of the electrode. For example, ReS_2-based composites were prepared by electrospinning and hydrothermal method, anchored ReS_2 nanosheets onto N-doped carbon nanofibers (N-CNFs) [99]. The large interlayer spacing and weak van der Waals interaction facilitate the easy diffusion of alkali metal ions. The carbon nanofibers can improve the electrical conductivity, and the doped nitrogen can adsorb sulfur and polysulfide generated from the conversion reaction. During the cycling, Li_2S_x, generated by the conversion reaction of ReS_2, will dissolve in the electrolyte, resulting in the loss of active substances. Therefore, the adsorption of sulfur and polysulfide prevents their aggregation and dissolution in the electrolyte, so as to play the stability of the cycle. The reversible capacity of ReS_2/N-CNFs remained 440 mAh·g^{-1} even after 400 cycles in LIBs at a current density of 100 mA·g^{-1}, more stable than other reported anodes based on ReS_2. Besides, the electrode made of ReS_2/CNTs composite in LIBs maintained a high capacity of 1048 mAh·g^{-1} at 0.2C (1C = 430 mA·g^{-1}), which is larger than that of bare-ReS_2 electrode [73]. The network of CNTs not only has a high conductive capacity and a large specific surface area, but also can organize the aggregation of active substances, thereby improving the performance of the composite electrode.

4.3.2 Catalytic electrode for water splitting

Since hydrogen is a green and environmentally friendly chemical fuel, hydrogen production from water splitting is of great interest. The electrolytic water splitting usually uses noble metals (e.g., platinum) as catalysts, which is resource-consuming and not cost-effective, making it unfavorable for sustainable development. TMDCs are potential candidates for the non-noble metal catalysts. The weak coupling of ReS_2 layers promotes the diffusion of electrolyte ions, and the weak interlayer coupling also exposes abundant edge sites, leading to better catalytic performance for ReS_2 as a catalyst in hydrogen evolution reaction (HER). The ReS_2/RGO hybrid, for example, has an onset potential of -100 mV (vs. RHE), a current density of -5.2 mA·cm^{-2} at -250 mV (vs. RHE), and a smaller Tafel slope of 107.4 mV·dec^{-1} than bare ReS_2, showing a better electrocatalytic activity for HER [74]. Additionally, introducing defects in ReS_2-based electrodes can improve the activity of catalysts, which not only presented a large number of active sites, but also reduced the free energy of hydrogen adsorption and enhanced the charge transfer efficiency. A carbon cloth loaded with Re/ ReS_2 nanosheets (Re/ReS_2/CC) exhibited noticeable electrocatalytic performance both in HER and OER [76]. The overpotentials of Re/ReS_2/CC electrode were 42 and 44 mV at 10 mA·cm^{-2} in acidic and alkaline conditions for HER, and the Tafel slopes were 36 and 53 mV·dec^{-1}, respectively. Under alkaline condition for OER, the overpotential was 290 mV at 10 mA·cm^{-2} and the Tafel slope was 81 mV·dec^{-1}, which was better than that of other ReS_2-based catalysts in the literature. The catalysts based on ReS_2 or its composites are expected to be an alternative to noble metal catalysts on account of its good stability, easy synthesis, and better catalytic performance.

5 Discussion and outlook

As a typical anisotropic 2D TMDC, ReS_2 maintains a twisted octahedron structure, whose anisotropic electrical and optical properties have been widely exploited in electronic and optoelectronic devices. Although the anisotropic structure and physical properties of ReS_2 can provide new perspectives and opportunities in the design of novel 2D functional devices, there are still many challenges in the practical applications of ReS_2.

First, the large-scale and controllable production of ReS_2 is still a problem, because of its complex structure. Compared with Mo in MoS_2, the abundance of Re on earth is quite low; therefore, the synthesis of ReS_2 is relatively costly. By adjusting the growth parameters in the chemical vapor deposition, large-size and high-quality single crystal

of ReS_2 can be achieved. However, the qualified synthetic sample may be obtained after constant exploration and summary of experiences. In addition, wet chemical synthesis method can fabricate a large quantity of samples with large size, but it suffers the uncontrollable layer numbers, which is mostly used in the field of energy storage. Moreover, the study of the growth mechanism of ReS_2 is still in the exploratory stage. The anisotropic growth mechanism needs to be proposed and validated.

Second, it is essential to rapidly identify the crystal axis for the utilization of the anisotropic performance in electronic or polarization-related devices. Consequently, designing an effective and nondestructive identification method is crucial. For example, angle-resolved Raman scattering spectroscopy, a polarization conductance measurement and angle-resolved polarization optical contrast spectroscopy provide not only methods for determining crystal orientation, but also important information for the quantitative analysis of the in-plane anisotropic optical properties of ReS_2 thin films. In a recent study, the anisotropic distribution of water droplets on the surface of 2D BP has been observed via optical microscopy, which can also be used to quickly identify the orientation of anisotropic structure in 2D materials [100].

Third, the quality of samples and the device repeatability are of vital importance in the electronic and optoelectronic applications. Intended for the quality of devices, many efforts have been made to promote the channel performance, including using post-treatment methods. For example, when an oxygen plasma treatment was applied on a thin-film transistor (TFT) of ReS_2, the mobility was increased by ~ 2 times and the off-current was decreased by a factor of 1×10^3, resulting in an enhanced on/off ratio of 1×10^4, compared with the pristine TFT [101]. It was also reported that a low-temperature thiol chemistry route can be used to repair sulfur vacancies in MoS_2 channels and improve the interface by reacting with (3-mercaptopropyl) trimethoxysilane (MPS). The method reduced the scattering from charged impurities and traps, thereby improving the carrier mobility of the device [102]. Therefore, pursuing a suitable and convenient post-treatment on the channel material has an important effect on the practical device applications.

Besides the channel material itself, the metal–semiconductor interface and the substrate supported the device greatly affect the carrier transport of devices based on 2D TMDCs. It is, therefore, essential to find suitable materials to reduce the height of the Schottky barrier at the metal–semiconductor interface and increase the efficiency of carrier injection [103]. Selecting the metal electrode with an appropriate work function may improve the Fermi level pinning effect, which makes the rational design of electronic and optical devices a feasible prospect. It has been

reported that the substrate also has a large influence on the modulation of the performance of 2D semiconductor devices [104, 105]. The interaction mechanisms between 2D semiconductor channel materials and the substrates are complicated, including the strain effect, charge transfer, dielectric screening, and light interference. Therefore, it is difficult to precisely control the interface interaction between the semiconductor and the substrate. The modulation of properties of 2D semiconductors by the substrate is still a new field in progress.

Finally, the device package and integration are very important for the practical application. The intrinsic properties of 2D materials with atomic thicknesses can easily be affected by the defects and impurities induced during the fabrication process of devices, resulting in a deterioration of device performance. A proper capping layer is indispensable to maintain the pristine performance. The integration of a single 2D device into the circuit is also a key issue. Furthermore, a higher degree and effectively vertical integration is one of the future directions in the electronic circuits based on 2D semiconductors. It has been shown that the unique lattice orientation of ReS₂ can be used as a design variable to adjust the transport characteristics of a 2D inverter [27]. Hence, the study of anisotropic materials can provide new ways for the optimization of electronic devices in future 2D integrated circuits.

In this review, we have summarized the characteristics of anisotropic ReS₂, which are different from other traditional isotropic 2D semiconductors due to its unique crystal structure. The anisotropic electrical, optical, and thermal properties along the different crystal directions in anisotropic ReS₂ can add new functions and optimize the performances of FETs, photodetectors, and thermal devices. Because ReS₂ is still a relatively new member of the 2D materials family, its intrinsic properties and exciting anisotropic applications call for further investigation. This review serves as an introduction to the exciting potential of ReS₂, and we also hope that it will stimulate the research interest on the anisotropic electrical and optical properties of 2D materials with a low lattice symmetry.

References

[1] Xie HC, Jiang SW, Shan J, Mak KF. Valley-selective exciton bistability in a suspended monolayer semiconductor. Nano Lett. 2018;18(5):3213.

[2] Zhang WD, Dong XA, Liang Y, Liu R, Sun YJ, Dong F. Synergetic effect of BiOCl/Bi₁₂O₁₇Cl₂ and MoS₂: in situ DRIFTS investigation on photocatalytic NO oxidation pathway. Rare Met. 2019;38(5):437.

[3] Mak KF, He K, Shan J, Heinz TF. Control of valley polarization in monolayer MoS₂ by optical helicity. Nat Nanotechnol. 2012;7(8):494.

[4] Zhao W, Ghorannevis Z, Chu L, Toh M, Kloc C, Tan PH, Eda G. Evolution of electronic structure in atomically thin sheets of WS₂ and WSe₂. ACS Nano. 2013;7(1):791.

[5] Wang QH, Kalantar-Zadeh K, Kis A, Coleman JN, Strano MS. Electronics and optoelectronics of two-dimensional transition metal dichalcogenides. Nat Nanotechnol. 2012;7(11):699.

[6] Mak KF, Lee C, Hone J, Shan J, Heinz TF. Atomically thin MoS₂: a new direct-gap semiconductor. Phys Rev Lett. 2010; 105(13):136805.

[7] Ding Y, Wang Y, Ni J, Shi L, Shi S, Tang W. First principles study of structural, vibrational and electronic properties of graphene-like MX₂ (M=Mo, Nb, W, Ta; X=S, Se, Te) monolayers. Phys B. 2011;406(11):2254.

[8] Lv R, Robinson JA, Schaak RE, Sun D, Sun Y, Mallouk TE, Terrones M. Transition metal dichalcogenides and beyond: synthesis, properties, and applications of single- and few-layer nanosheets. Acc Chem Res. 2015;48(1):56.

[9] Zhang X, Zhao HB, Zhang QZ, Wei F. Controllable growth and morphology evolution of 2D MoS₂ via CVD method. Chin J Rare Met. 2020;44(12):1249.

[10] Geim AK, Novoselov KS. The rise of graphene. Nat Mater. 2007;6(3):183.

[11] Choi W, Choudhary N, Han GH, Park J, Akinwande D, Lee YH. Recent development of two-dimensional transition metal dichalcogenides and their applications. Mater Today. 2017; 20(3):116.

[12] Li H, Wu J, Yin Z, Zhang H. Preparation and applications of mechanically exfoliated single-layer and multilayer MoS₂ and WSe₂ nanosheets. Acc Chem Res. 2014;47(4):1067.

[13] Zhao S, Dong B, Wang H, Wang H, Zhang Y, Han ZV, Zhang H. In-plane anisotropic electronics based on low-symmetry 2D materials: progress and prospects. Nanoscale Advances. 2020; 2(1):109.

[14] Ling X, Wang H, Huang S, Xia F, Dresselhaus MS. The renaissance of black phosphorus. Proc Natl Acad Sci USA. 2015;112(15):4523.

[15] Xia F, Wang H, Jia Y. Rediscovering black phosphorus as an anisotropic layered material for optoelectronics and electronics. Nat Commun. 2014;5(1):4458.

[16] Qiao J, Kong X, Hu ZX, Yang F, Ji W. High-mobility transport anisotropy and linear dichroism in few-layer black phosphorus. Nat Commun. 2014;5:4475.

[17] Zhang S, Yang J, Xu R, Wang F, Li W, Ghufran M, Zhang YW, Yu Z, Zhang G, Qin Q, Lu Y. Extraordinary photoluminescence and strong temperature/angle-dependent raman responses in few-layer phosphorene. ACS Nano. 2014;8(9): 9590.

[18] Wei Q, Peng X. Superior mechanical flexibility of phosphorene and few-layer black phosphorus. Appl Phys Lett. 2014; 104(25):251915.

[19] Wang Z, Jia H, Zheng XQ, Yang R, Ye GJ, Chen XH, Feng PX. Resolving and tuning mechanical anisotropy in black phosphorus via nanomechanical multimode resonance spectromicroscopy. Nano Lett. 2016;16(9):5394.

[20] Wang X, Jones AM, Seyler KL, Tran V, Jia Y, Zhao H, Wang H, Yang L, Xu X, Xia F. Highly anisotropic and robust excitons in monolayer black phosphorus. Nat Nanotechnol. 2015; 10(6):517.

[21] Castellanos-Gomez A. Black phosphorus: narrow gap, wide applications. J Phys Chem Lett. 2015;6(21):4280.

[22] Nam GH, He Q, Wang X, Yu Y, Chen J, Zhang K, Yang Z, Hu D, Lai Z, Li B, Xiong Q, Zhang Q, Gu L, Zhang H. In-plane anisotropic properties of 1T′-MoS₂ layers. Adv Mater. 2019; 31(21):1807764.

[23] Zhao H, Wu J, Zhong H, Guo Q, Wang X, Xia F, Yang L, Tan P, Wang H. Interlayer interactions in anisotropic atomically thin rhenium diselenide. Nano Res. 2015;8(11):3651.

[24] Wolverson D, Crampin S, Kazemi AS, Ilie A, Bending SJ. Raman spectra of monolayer, few-layer, and bulk ReSe₂: an anisotropic layered semiconductor. ACS Nano. 2014;8(11): 11154.

[25] Hart L, Dale S, Hoye S, Webb JL, Wolverson D. Rhenium dichalcogenides: layered semiconductors with two vertical orientations. Nano Lett. 2016;16(2):1381.

[26] Tongay S, Sahin H, Ko C, Luce A, Fan W, Liu K, Zhou J, Huang YS, Ho CH, Yan J, Ogletree DF, Aloni S, Ji J, Li S, Li J, Peeters FM, Wu J. Monolayer behaviour in bulk ReS₂ due to electronic and vibrational decoupling. Nat Commun. 2014;5: 3252.

[27] Liu E, Fu Y, Wang Y, Feng Y, Liu H, Wan X, Zhou W, Wang B, Shao L, Ho CH, Huang YS, Cao Z, Wang L, Li A, Zeng J, Song F, Wang X, Shi Y, Yuan H, Hwang HY, Cui Y, Miao F, Xing D. Integrated digital inverters based on two-dimensional anisotropic ReS₂ field-effect transistors. Nat Commun. 2015;6: 6991.

[28] Wang R, Yu Y, Zhou S, Li H, Wong H, Luo Z, Gan L, Zhai T. Strategies on phase control in transition metal dichalcogenides. Adv Func Mater. 2018;28(47):1802473.

[29] Chhowalla M, Shin HS, Eda G, Li LJ, Loh KP, Zhang H. The chemistry of two-dimensional layered transition metal dichalcogenide nanosheets. Nat Chem. 2013;5(4):263.

[30] Shi J, Yu P, Liu F, He P, Wang R, Qin L, Zhou J, Li X, Zhou J, Sui X, Zhang S, Zhang Y, Zhang Q, Sum TC, Qiu X, Liu Z, Liu X. 3R MoS₂ with broken inversion symmetry: a promising ultrathin nonlinear optical device. Adv Mater. 2017;29(30): 1701486.

[31] Qi Y, Naumov PG, Ali MN, Rajamathi CR, Schnelle W, Barkalov O, Hanfland M, Wu SC, Shekhar C, Sun Y, Suss V, Schmidt M, Schwarz U, Pippel E, Werner P, Hillebrand R, Forster T, Kampert E, Parkin S, Cava RJ, Felser C, Yan B, Medvedev SA. Superconductivity in Weyl semimetal candidate MoTe₂. Nat Commun. 2016;7:11038.

[32] Voiry D, Mohite A, Chhowalla M. Phase engineering of transition metal dichalcogenides. Chem Soc Rev. 2015;44(9): 2702.

[33] Lee C, Yan H, Brus LE, Heinz TF, Hone J, Ryu S. Anomalous lattice vibrations of single- and few-layer MoS₂. ACS Nano. 2010;4(5):2695.

[34] Yu ZG, Cai Y, Zhang YW. Robust direct bandgap characteristics of one- and two-dimensional ReS₂. Sci Rep. 2015;5(1): 13783.

[35] Feng Y, Zhou W, Wang Y, Zhou J, Liu E, Fu Y, Ni Z, Wu X, Yuan H, Miao F, Wang B, Wan X, Xing D. Raman vibrational spectra of bulk to monolayer ReS₂ with lower symmetry. Phys Rev B, 2015; 92(5):054110.

[36] Xiong Y, Chen HW, Zhang DW, Zhou P. Electronic and optoelectronic applications based on ReS₂. Phys Status Solidi Rapid Res Lett. 2019;13(6):1800658.

[37] Yun WS, Han S, Hong SC, Kim IG, Lee J. Thickness and strain effects on electronic structures of transition metal dichalcogenides: 2H-MX₂ semiconductors (M= Mo, W; X= S, Se, Te). Phys Rev B. 2012;85(3):033305.

[38] Kuc A, Zibouche N, Heine T. Influence of quantum confinement on the electronic structure of the transition metal sulfide TS₂. Phys Rev B. 2011;83(24):245213.

[39] Splendiani A, Sun L, Zhang Y, Li T, Kim J, Chim CY, Galli G, Wang F. Emerging photoluminescence in monolayer MoS₂. Nano Lett. 2010;10(4):1271.

[40] Park JY, Joe HE, Yoon HS, Yoo S, Kim T, Kang K, Min BK, Jun SC. Contact effect of ReS₂/metal interface. ACS Appl Mater Interfaces. 2017;9(31):26325.

[41] Aslan OB, Chenet DA, van der Zande AM, Hone JC, Heinz TF. Linearly polarized excitons in single- and few-layer ReS₂ crystals. ACS Photonics. 2015;3(1):96.

[42] Zhang E, Jin Y, Yuan X, Wang W, Zhang C, Tang L, Liu S, Zhou P, Hu W, Xiu F. ReS₂-based field-effect transistors and photodetectors. Adv Func Mater. 2015;25(26):4076.

[43] Cui Q, He J, Bellus MZ, Mirzokarimov M, Hofmann T, Chiu HY, Antonik M, He D, Wang Y, Zhao H. Transient absorption measurements on anisotropic monolayer ReS₂. Small. 2015; 11(41):5565.

[44] Wang YY, Zhou JD, Jiang J, Yin TT, Yin ZX, Liu Z, Shen ZX. In-plane optical anisotropy in ReS₂ flakes determined by angle-resolved polarized optical contrast spectroscopy. Nanoscale. 2019;11(42):20199.

[45] Zhang X, Qiao XF, Shi W, Wu JB, Jiang DS, Tan PH. Phonon and Raman scattering of two-dimensional transition metal dichalcogenides from monolayer, multilayer to bulk material. Chem Soc Rev. 2015;44(9):2757.

[46] Nagler P, Plechinger G, Schüller C, Korn T. Observation of anisotropic interlayer Raman modes in few-layer ReS₂, physica status solidi. RRL Rapid Res Lett. 2016;10(2):185.

[47] Lorchat E, Froehlicher G, Berciaud S. Splitting of interlayer shear modes and photon energy dependent anisotropic raman response in N-layer ReSe₂ and ReS₂. ACS Nano. 2016;10(2):2752.

[48] He R, Yan JA, Yin Z, Ye Z, Ye G, Cheng J, Li J, Lui CH. Coupling and stacking order of ReS₂ atomic layers revealed by ultralow-frequency raman spectroscopy. Nano Lett. 2016; 16(2):1404.

[49] Liang L, Zhang J, Sumpter BG, Tan QH, Tan PH, Meunier V. Low-frequency shear and layer-breathing modes in raman scattering of two-dimensional materials. ACS Nano. 2017; 11(12):11777.

[50] Zhao Y, Luo X, Li H, Zhang J, Araujo PT, Gan CK, Wu J, Zhang H, Quek SY, Dresselhaus MS, Xiong Q. Interlayer breathing and shear modes in few-trilayer MoS₂ and WSe₂. Nano Lett. 2013;13(3):1007.

[51] Zhang X, Han WP, Wu JB, Milana S, Lu Y, Li QQ, Ferrari AC, Tan PH. Raman spectroscopy of shear and layer breathing modes in multilayer MoS₂. Phys Rev B. 2013;87(11):115413.

[52] Boukhicha M, Calandra M, Measson MA, Lancry O, Shukla A. Anharmonic phonons in few-layer MoS₂: Raman spectroscopy of ultralow energy compression and shear modes. Phys Rev B. 2013;87(19):195316.

[53] Ferrari AC, Basko DM. Raman spectroscopy as a versatile tool for studying the properties of graphene. Nat Nanotechnol. 2013;8(4):235.

[54] Ling X, Huang S, Hasdeo EH, Liang L, Parkin WM, Tatsumi Y, Nugraha ART, Puretzky AA, Das PM, Sumpter BG, Geohegan DB, Kong J, Saito R, Drndic M, Meunier V, Dresselhaus MS. Anisotropic electron-photon and electron-phonon interactions in black phosphorus. Nano Lett. 2016;16(4):2260.

[55] Ribeiro HB, Pimenta MA, de Matos CJS, Moreira RL, Rodin AS, Zapata JD, de Souza EAT, CastroNeto AH. Unusual angular dependence of the Raman response in black phosphorus. ACS Nano. 2015;9(4):4270.

[56] Song Q, Pan X, Wang H, Zhang K, Tan Q, Li P, Wan Y, Wang Y, Xu X, Lin M, Wan X, Song F, Dai L. The in-plane anisotropy of WTe₂ investigated by angle-dependent and polarized Raman spectroscopy. Sci Rep. 2016;6(1):29254.

[57] Tian Z, Guo C, Zhao M, Li R, Xue J. Two-dimensional SnS: a phosphorene analogue with strong in-plane electronic anisotropy. ACS Nano. 2017;11(2):2219.

[58] Zhang S, Mao N, Zhang N, Wu J, Tong L, Zhang J. Anomalous polarized Raman scattering and large circular intensity differential in layered triclinic ReS$_2$. ACS Nano. 2017;11(10):10366.

[59] Chenet DA, Aslan OB, Huang PY, Fan C, van der Zande AM, Heinz TF, Hone JC. In-plane anisotropy in mono- and few-layer ReS$_2$ probed by Raman spectroscopy and scanning transmission electron microscopy. Nano Lett. 2015;15(9):5667.

[60] Jang H, Ryder CR, Wood JD, Hersam MC, Cahill DG. 3D anisotropic thermal conductivity of exfoliated rhenium disulfide. Adv Mater. 2017;29(35):1700650.

[61] Jariwala B, Voiry D, Jindal A, Chalke BA, Bapat R, Thamizhavel A, Chhowalla M, Deshmukh M, Bhattacharya A. Synthesis and characterization of ReS$_2$ and ReSe$_2$ layered chalcogenide single crystals. Chem Mater. 2016;28(10):3352.

[62] Rahman M, Davey K, Qiao SZ. Advent of 2D rhenium disulfide (ReS$_2$): fundamentals to applications. Adv Func Mater. 2017;27(10):1606129.

[63] Coleman JN, Lotya M, O'Neill A, Bergin SD, King PJ, Khan U, Young K, Gaucher A, De S, Smith RJ, Shvets IV, Arora SK, Stanton G, Kim HY, Lee K, Kim GT, Duesberg GS, Hallam T, Boland JJ, Wang JJ, Donegan JF, Grunlan JC, Moriarty G, Shmeliov A, Nicholls RJ, Perkins JM, Grieveson EM, Theuwissen K, McComb DW, Nellist PD, Nicolosi V. Two-dimensional nanosheets produced by liquid exfoliation of layered materials. Science. 2011;331:568.

[64] Fujita T, Ito Y, Tan Y, Yamaguchi H, Hojo D, Hirata A, Voiry D, Chhowalla M, Chen M. Chemically exfoliated ReS$_2$ nanosheets. Nanoscale. 2014;6(21):12458.

[65] Coleman JN. Liquid exfoliation of defect-free graphene. Acc Chem Res. 2013;46(1):14.

[66] Qi F, Chen Y, Zheng B, Zhou J, Wang X, Li P, Zhang W. Facile growth of large-area and high-quality few-layer ReS$_2$ by physical vapour deposition. Mater Lett. 2016;184:324.

[67] He X, Liu F, Hu P, Fu W, Wang X, Zeng Q, Zhao W, Liu Z. Chemical vapor deposition of high-quality and atomically layered ReS$_2$. Small. 2015;11(40):5423.

[68] Keyshar K, Gong Y, Ye G, Brunetto G, Zhou W, Cole DP, Hackenberg K, He Y, Machado L, Kabbani M, Hart AH, Li B, Galvao DS, George A, Vajtai R, Tiwary CS, Ajayan PM. Chemical vapor deposition of monolayer rhenium disulfide (ReS$_2$). Adv Mater. 2015;27(31):4640.

[69] Cui F, Wang C, Li X, Wang G, Liu K, Yang Z, Feng Q, Liang X, Zhang Z, Liu S, Lei Z, Liu Z, Xu H, Zhang J. Tellurium-assisted epitaxial growth of large-area, highly crystalline ReS$_2$ atomic layers on mica substrate. Adv Mater. 2016;28(25):5019.

[70] Kim Y, Kang B, Choi Y, Cho JH, Lee C. Direct synthesis of large-area continuous ReS$_2$ films on a flexible glass at low temperature. 2D Mater. 2017;4(2):025057.

[71] He Q, Zhou J, Tang W, Hao Y, Sun L, Zhu C, Xu F, Chen J, Wu Y, Wu Z, Xu B, Liu G, Li X, Zhang C, Kang J. Deeply exploring anisotropic evolution toward large-scale growth of monolayer ReS$_2$. ACS Appl Mater Interfaces. 2020;12(2):2862.

[72] Li X, Wang X, Hong J, Liu D, Feng Q, Lei Z, Liu K, Ding F, Xu H. Nanoassembly growth model for subdomain and grain boundary formation in 1T′ layered ReS$_2$. Adv Func Mater. 2019;29(49):1906385.

[73] Qi F, He J, Chen Y, Zheng B, Li Q, Wang X, Yu B, Lin J, Zhou J, Li P, Zhang W, Li Y. Few-layered ReS$_2$ nanosheets grown on carbon nanotubes: a highly efficient anode for high-performance lithium-ion batteries. Chem Eng J. 2017;315:10.

[74] Gao H, Yue HH, Qi F, Yu B, Zhang WL, Chen YF. Few-layered ReS$_2$ nanosheets grown on graphene as electrocatalyst for hydrogen evolution reaction. Rare Met. 2018;37(12):1014.

[75] Wang H, Jiang X, Yang X, Yu Z, Yuan R. Fluffy carbon-coated ReS$_2$ nanoflowers as enhanced anode materials for lithium ion battery. Mater Chem Phys. 2019;232:506.

[76] Pang QQ, Niu ZL, Yi SS, Zhang S, Liu ZY, Yue XZ, Hydrogen-etched bifunctional sulfur-defect-rich ReS$_2$/CC electrocatalyst for highly efficient HER and OER. Small. 2020;16(34):2003007.

[77] Xie X, Mao M, Qi S, Ma J. ReS$_2$-based electrode materials for alkali-metal ion batteries. CrystEngComm. 2019;21(25):3755.

[78] Liu S, Liu Y, Lei W, Zhou X, Xu K, Qiao Q, Zhang WH. Few-layered ReS$_2$ nanosheets vertically aligned on reduced graphene oxide for superior lithium and sodium storage. J Mater Chem A. 2018;6(41):20267.

[79] Wu M, Yang J, Ng DHL, Ma J. Rhenium diselenide anchored on reduced graphene oxide as anode with cyclic stability for potassium-ion battery, physica status solidi. RRL Rapid Res Lett. 2019;13(10):1900329.

[80] Long M, Wang P, Fang H, Hu W. Progress, challenges, and opportunities for 2D material based photodetectors. Adv Func Mater. 2018;29(19):1803807.

[81] Liu F, Zheng S, He X, Chaturvedi A, He J, Chow WL, Mion TR, Wang X, Zhou J, Fu Q, Fan HJ, Tay BK, Song L, He RH, Kloc C, Ajayan PM, Liu Z. Highly sensitive detection of polarized light using anisotropic 2D ReS$_2$. Adv Func Mater. 2016;26(8):1169.

[82] Gong C, Zhang Y, Chen W, Chu J, Lei T, Pu J, Dai L, Wu C, Cheng Y, Zhai T, Li L, Xiong J. Electronic and optoelectronic applications based on 2D novel anisotropic transition metal dichalcogenides. Adv Sci (Weinh). 2017;4(12):1700231.

[83] Zhao J, Ma D, Wang C, Guo Z, Zhang B, Li J, Nie G, Xie N, Zhang H. Recent advances in anisotropic two-dimensional materials and device applications. Nano Res. 2020;14(4):897.

[84] Yu WJ, Li Z, Zhou H, Chen Y, Wang Y, Huang Y, Duan X. Vertically stacked multi-heterostructures of layered materials for logic transistors and complementary inverters. Nat Mater. 2013;12(3):246.

[85] Yu WJ, Liu Y, Zhou H, Yin A, Li Z, Huang Y, Duan X. Highly efficient gate-tunable photocurrent generation in vertical heterostructures of layered materials. Nat Nanotechnol. 2013;8(12):952.

[86] Liu Y, Huang Y, Duan X, Vander D. Waals integration before and beyond two-dimensional materials. Nature. 2019;567(7748):323.

[87] Wang FK, Zhai TY. Towards scalable van der Waals heterostructure arrays. Rare Met. 2020;39(4):327.

[88] Mukherjee B, Zulkefli A, Hayakawa R, Wakayama Y, Nakaharai S. Enhanced quantum efficiency in vertical mixed-thickness n-ReS$_2$/p-Si heterojunction photodiodes. ACS Photonics. 2019;6(9):2277.

[89] Kang B, Kim Y, Yoo WJ, Lee C. Ultrahigh photoresponsive device based on ReS$_2$/graphene heterostructure. Small. 2018;14(45):1802593.

[90] Cao S, Xing Y, Han J, Luo X, Lv W, Lv W, Zhang B, Zeng Z. Ultrahigh-photoresponsive UV photodetector based on a BP/ReS$_2$ heterostructure p-n diode. Nanoscale. 2018;10(35):16805.

[91] Zhao M, Zhang W, Liu M, Zou C, Yang K, Yang Y, Dong Y, Zhang L, Huang S. Interlayer coupling in anisotropic/isotropic van der Waals heterostructures of ReS$_2$ and MoS$_2$ monolayers. Nano Res. 2016;9(12):3772.

[92] Liu DY, Hong JH, Wang X, Li XB, Feng QL, Tan CW, Zhai TY, Ding F, Peng HL, Xu H. Diverse atomically sharp

interfaces and linear dichroism of 1T′ ReS₂-ReSe₂ lateral p-n heterojunctions. Adv Func Mater. 2018;28(47):1804696.

[93] Yan R, Fathipour S, Han Y, Song B, Xiao S, Li M, Ma N, Protasenko V, Muller DA, Jena D, Xing HG. Esaki diodes in van der Waals heterojunctions with broken-gap energy band alignment. Nano Lett. 2015;15(9):5791.

[94] Roy T, Tosun M, Cao X, Fang H, Lien DH, Zhao P, Chen YZ, Chueh YL, Guo J, Javey A. Dual-gated MoS₂/WSe₂ van der Waals tunnel diodes and transistors. ACS Nano. 2015;9(2):2071.

[95] Nourbakhsh A, Zubair A, Dresselhaus MS, Palacios T. Transport properties of a MoS₂/WSe₂ heterojunction transistor and its potential for application. Nano Lett. 2016;16(2):1359.

[96] Shim J, Oh S, Kang DH, Jo SH, Ali MH, Choi WY, Heo K, Jeon J, Lee S, Kim M, Song YJ, Park JH. Phosphorene/rhenium disulfide heterojunction-based negative differential resistance device for multi-valued logic. Nat Commun. 2016;7:13413.

[97] Xiong X, Kang J, Hu Q, Gu C, Gao T, Li X, Wu Y. Reconfigurable logic-in-memory and multilingual artificial synapses based on 2d heterostructures. Adv Func Mater. 2020;30(11):1909645.

[98] Zhang Q, Tan S, Mendes RG, Sun Z, Chen Y, Kong X, Xue Y, Rümmeli MH, Wu X, Chen S, Fu L. Extremely weak van der Waals coupling in vertical ReS₂ nanowalls for high-current-density lithium-ion batteries. 2016;28(13):2616.

[99] Mao ML, Cui CY, Wu MG, Zhang M, Gao T, Fan XL, Chen J, Wang TH, Ma JM, Wang CS. Flexible ReS₂ nanosheets/N-doped carbon nanofibers-based paper as a universal anode for alkali (Li, Na, K) ion battery. Nano Energy. 2018;45:346.

[100] Zhao J, Zhu J, Cao R, Wang H, Guo Z, Sang DK, Tang J, Fan D, Li J, Zhang H. Liquefaction of water on the surface of anisotropic two-dimensional atomic layered black phosphorus. Nat Commun. 2019;10(1):4062.

[101] Shim J, Oh A, Kang DH, Oh S, Jang SK, Jeon J, Jeon MH, Kim M, Choi C, Lee J, Lee S, Yeom GY, Song YJ, Park JH. High-performance 2D rhenium disulfide (ReS₂) transistors and photodetectors by oxygen plasma treatment, 2016;28(32):6985.

[102] Yu Z, Pan Y, Shen Y, Wang Z, Ong ZY, Xu T, Xin R, Pan L, Wang B, Sun L, Wang J, Zhang G, Zhang YW, Shi Y, Wang X. Towards intrinsic charge transport in monolayer molybdenum disulfide by defect and interface engineering. Nat Commun. 2014;5:5290.

[103] Gao N, Zhou S, Liu N, Bai Y, Zhao J. Selecting electrode materials for monolayer ReS₂ with an Ohmic contact. J Mater Chem C. 2018;6(25):6764.

[104] Sun YH, Wang RM, Liu K. Substrate induced changes in atomically thin 2-dimensional semiconductors: fundamentals, engineering, and applications. Appl Phys Rev. 2017;4(1):011301.

[105] Nazir G, Rehman MA, Khan MF, Dastgeer G, Aftab S, Afzal AM, Seo Y, Eom J. Comparison of electrical and photoelectrical properties of ReS₂ field-effect transistors on different dielectric substrates. ACS Appl Mater Interfaces. 2018;10(38):32501.
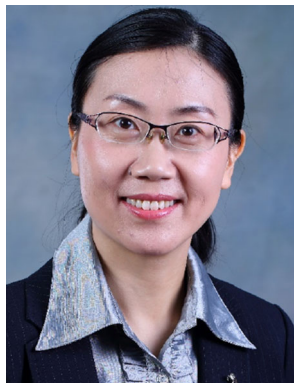
Yinghui Sun obtained her BS degree (2003) in Applied Physics from Xi'an Jiaotong University and Ph.D. degree (2008) in Physics from Tsinghua University. She started as an assistant Professor in the University of Science and Technology Beijing in 2015, and was promoted to associate Professor in 2017. Her current research focuses on the characterization and application of composite systems of metal nanoparticles and two-dimensional materials.

Rong-Ming Wang received his Bachelor and Master's degrees in Physics from Peking University and Ph.D. degree in Materials Science from Beijing Institute of Aeronautical Materials, China. In 2004–2005, he was a visiting scholar in University of California, Berkeley. Then, he joined Beihang University as a Professor in Physics. Currently, he is a professor in University of Science and Technology Beijing, Director of Beijing Key Laboratory for Magneto-Photoelectrical Composite and Interface Science and Team Leaders for Advanced Functional Material, Beijing Advanced Innovation Center of Materials Genome Engineering. His research interests include magnetic nanomaterial, transmission electron microscopy, interface science, and materials genome engineering.